

Revealing the higher-order spin nature of the Hall
effect in non-collinear antiferromagnet
 $\text{Mn}_3\text{Ni}_{0.35}\text{Cu}_{0.65}\text{N}$

Adithya Rajan¹, Tom G. Saunderson^{1,2}, Fabian R. Lux^{1,2,3},
Rocío Yanes Díaz⁴, Hasan M. Abdullah⁵, Arnab Bose¹,
Beatrice Bednarz¹, Jun-Young Kim^{1,6}, Dongwook Go^{1,2},
Tetsuya Hajiri⁷, Gokaran Shukla⁵, Olena Gomonay¹, Yugui Yao⁸,
Wanxiang Feng⁸, Hidefumi Asano⁷, Udo Schwingenschlög⁵,
Luis López-Díaz⁴, Jairo Sinova¹, Yuriy Mokrousov^{1,2},
Aurélien Manchon⁹, Mathias Kläui^{1,10*}

¹Institute of Physics, Johannes Gutenberg-University Mainz,
Staudingerweg 7, Mainz, 55128, Germany.

²Peter Grünberg Institut and Institute for Advanced Simulation,
Forschungszentrum Jülich and JARA, Jülich, 52425, Germany.

³Department of Physics, Yeshiva University, , New York, NY, USA.

⁴Department of Applied Physics, Universidad de Salamanca, Plaza de la
Merced, Salamanca, 37008, Spain.

⁵Physical Science and Engineering Division, King Abdullah University
of Science and Technology, Thuwal, 23955-6900, Saudi Arabia.

⁶Institute of Materials Research and Engineering (IMRE), Agency for
Science, Technology and Research (A*STAR), Singapore, 138634,
Singapore.

⁷Department of Materials Physics, Nagoya University, Nagoya,
464-8603, Japan.

⁸Beijing Institute of Technology, Beijing, 100081, China.

⁹Aix-Marseille Université, CNRS, CINaM, Marseille, France.

¹⁰Centre for Quantum Spintronics, Norwegian University of Science and
Technology, Trondheim, 7491, Norway.

*Corresponding author(s). E-mail(s): klaeui@uni-mainz.de;

Abstract

Ferromagnets generate an anomalous Hall effect even without the presence of a magnetic field, something that conventional antiferromagnets cannot replicate but noncollinear antiferromagnets can. The anomalous Hall effect governed by the resistivity tensor plays a crucial role in determining the presence of time reversal symmetry and the topology present in the system. In this work we reveal the complex origin of the anomalous Hall effect arising in noncollinear antiferromagnets by performing Hall measurements with fields applied in selected directions in space with respect to the crystalline axes. Our coplanar magnetic field geometry goes beyond the conventional perpendicular field geometry used for ferromagnets and allows us to suppress any magnetic dipole contribution. It allows us to map the in-plane anomalous Hall contribution and we demonstrate a 120° symmetry which we find to be governed by the octupole moment at high fields. At low fields we subsequently discover a surprising topological Hall-like signature and, from a combination of theoretical techniques, we show that the spins can be recast into dipole, emergent octupole and noncoplanar effective magnetic moments. These co-existing orders enable magnetization dynamics unachievable in either ferromagnetic or conventional collinear antiferromagnetic materials.

Keywords: Anomalous Hall effect, Noncollinear Antiferromagnets, Spintronics, Berry curvature

1 Introduction

Broken time reversal symmetry (\mathcal{T}) and its interplay with the spin-orbit coupling (SOC) result in the transverse flow of electrons generating an anomalous Hall voltage, a signature that distinguishes a ferromagnet (FM) from conventional antiferromagnets (AFM) [1, 2]. However, it has been predicted that a certain class of AFMs with noncollinear spin textures can lead to an unusual type of anomalous Hall effect (AHE) that can exist even in the absence of a net magnetization due to spin-lattice coupling [3, 4]. Whilst in noncollinear antiferromagnets (NC-AFM) it has been shown that their weak magnetization is insufficient to account for the AHE [5–9], further work to experimentally substantiate the fundamental mechanism responsible for the observed AHE signals has still not been undertaken. This is because any studies of the AHE have, so far, only been performed with the electrical measurements in plane while driving a magnetic field out of the plane, entangling the magnetization signal to any novel contribution to the AHE. In order to understand the origin of the AHE signal, one must go beyond the perpendicular field geometry and apply the field in different directions in space to identify the symmetry, and from this the mechanism leading to the AHE signal. Here we show the full dependence of the AHE in the NC-AFM $\text{Mn}_3\text{Ni}_{0.35}\text{Cu}_{0.65}\text{N}$ (Mn_3NiCuN) when the magnetic field is swept not only out-of-plane but also in the plane. The in-plane field experimental configuration, by construction, does not allow for the conventional dipole (magnetization) component of the AHE signal to contribute. We can therefore show, using a variety of theoretical techniques, that at high fields the in-plane AHE comes purely from the octupole moment and,

surprisingly, an additional topological Hall-like (THE) signal occurs at low fields. Our results demonstrate that in NC-AFMs one must expand beyond the dipole contribution to the AHE to explain their rich, coexisting orders. Such coexisting orders go beyond the magnetization dynamics achievable in conventional FMs and AFMs. Harnessing these coexisting orders paves the way for spintronic devices that go beyond the state-of-the-art.

The antisymmetric AHE in the NC-AFM arises from the octupole moment produced by the noncollinear frustrated spin structure in the kagome plane [3, 10] which is in the (111) plane in the case of Mn_3NiCuN , the material we are investigating in this work (Fig. 1(a)). This can be visualized as an emergent octupole moment [10–16], $\vec{Q}_{T_{1g}}$ (the first term in equation (1)) that purely originates from the coplanar orientation of the spin texture lying in the kagome plane (Fig. 1(a)). In Mn_3NiCuN , the direction of $\vec{Q}_{T_{1g}}$ points out of the kagome plane, along [111] direction. Upon expanding the AHE signal in the local spins, beyond the conventional ferromagnetic case, the octupole and topological Hall effects [17–20] emerge as higher order contributions to the Hall effect in noncollinear compounds. Hence, the total contributions to the AHE are,

$$\sigma_{xy} = \gamma_{\text{Oct}} \left[\vec{Q}_{T_{1g}} \right]_z + \gamma_{\text{dip}} \left[\vec{M}_{T_{1g}} \right]_z + \gamma_{\text{SSC}} \left[\sum_{ijk} \vec{S}_i \cdot (\vec{S}_j \times \vec{S}_k) \right], \quad (1)$$

where equation (1) is obtained by using representation theory to derive the irreducible representations of Mn_3NiCuN as described in section ‘2 Representation theory’ of the supplementary material [21]. The second term of equation (1) represents the conventional AHE, proportional to the net magnetic dipole moment, $\vec{M}_{T_{1g}}$, as observed in a regular ferromagnet such as Fe [1], and that can arise in our system due to the canting of the spins upon the application of an external magnetic field. Generally, in this type of NC-AFM [22], including our system (see Fig. S2(a) in ‘1.1 Sample characterization’ [21]), the induced moment is very small [22] and therefore has a very small effect on the AHE.

Equation (1) predicts that $\vec{Q}_{T_{1g}}$ produces the maximum AHE when the magnetic field is swept out of the plane while the electrical measurements are performed in the kagome plane. This arrangement is similar to the measurement of AHE in a regular ferromagnet (FM) where the direction of the applied electric current (J_{xx}), voltage measurement (V_{xy}) and magnetic moment (M_z) are orthogonal to each other ($V_{xy} \propto (J_{xx}M_z)$). Alternatively, in NC-AFMs with a vanishing magnetic moment, $\vec{Q}_{T_{1g}}$ plays the role of a fictitious magnetization, akin to M_z in ferromagnets. Nonetheless our symmetry analysis reveals a fundamental difference between the octupole driven AHE and the conventional dipole driven AHE: the magnetic octupole supports a specific finite AHE response when the external field is rotated *in the plane* of the electrical measurements, whereas the dipole driven AHE remains unaffected. Thus, in plane fields have to be used to reveal this contribution.

The octupole vector $\vec{Q}_{T_{1g}}$ hosts a total of eight poles in Mn_3NiCuN as shown with the grey vectors in Fig. 1(b), two of which point out of the plane, along the [111] direction and six others have projections both in the plane and out of the plane with 120° in-plane rotational symmetry enforced by the crystal structure (space group $Pm\bar{3}m$

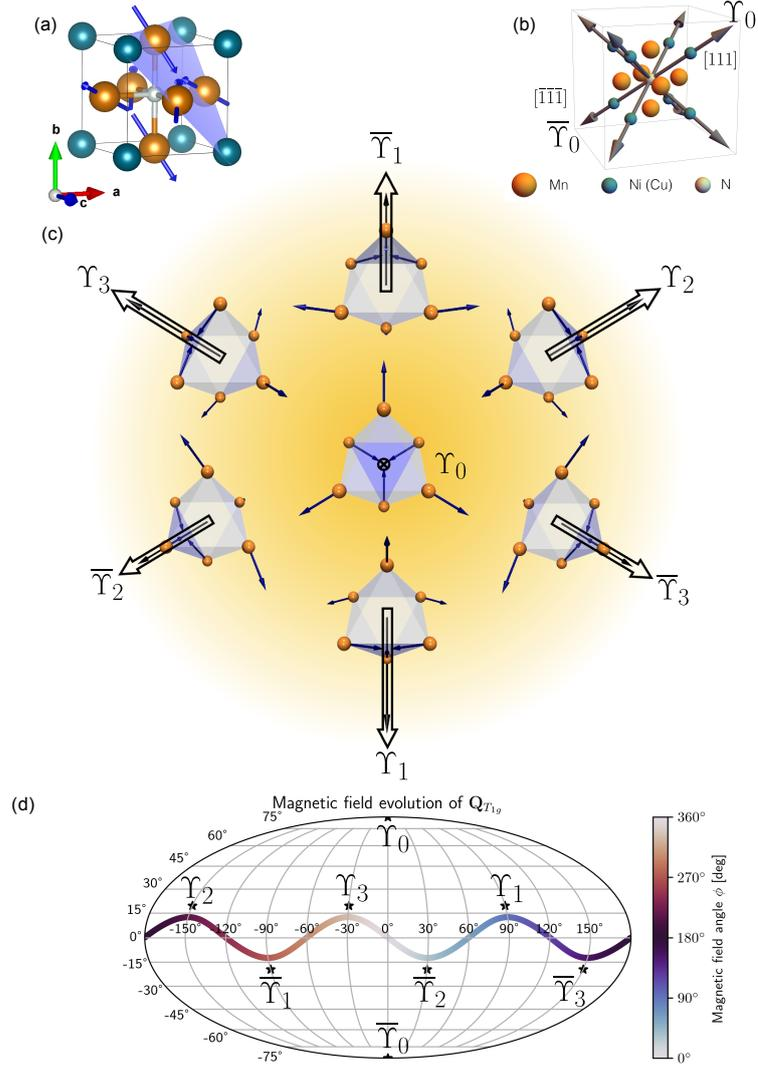


Fig. 1 Cubic unit cell of Mn₃NiCuN with Mn atoms in orange, Ni and Cu in blue, and N in off-white. The blue arrows in (a) indicate the Mn spin arrangement in the (111) plane (blue). (b) The eight octupoles which point perpendicular to the 8 equivalent (111) planes. The out-of-plane components of the octupole moment are labelled as Υ_0 and $\bar{\Upsilon}_0$, pointing along the [111] and $[\bar{1}\bar{1}\bar{1}]$ directions respectively. (c) The Mn spin configurations (blue arrows) and the corresponding octupoles (black bold arrows) when a magnetic field is applied along different crystallographic directions in the (111) plane. The particular directions labelled represent the specific angles where the magnetic field is parallel to the in-plane projections of the octupoles Υ_i and $\bar{\Upsilon}_i$. The central panel of (c) shows the spin configuration when the magnetic field is swept out the kagome plane ($\bar{\Upsilon}_0$) and that corresponds to $\vec{Q}_{T_{1g}}$ along [111] direction. (d) Graphical representation of the evolution of $\vec{Q}_{T_{1g}}$ in spherical coordinates as a function of the applied external magnetic field in the (111) Kagome plane (shown in color bar). It shows 120° oscillations of the projection of $\vec{Q}_{T_{1g}}$ along [111] direction, parallel to the Υ_0 octupole. When the magnetic field is swept from positive to negative in-plane field along certain in-plane projections of the octupole, for example Υ_1 to $\bar{\Upsilon}_1$, there is switching of the out-of-plane component of $\vec{Q}_{T_{1g}}$ with the maximum strength (shown in black stars), which will manifest as a step in the Hall resistance (generating AHE) and follow 120° angular dependence.

(No. 221), point group $m\bar{3}m$ (O_h)). It is evident that when an external field is applied out-of-plane, along the [111] axis, one expects to obtain an AHE from the combination of octupole ($\vec{Q}_{T_{1g}}$) and dipole ($\vec{M}_{T_{1g}}$) contributions. However, our symmetry analysis additionally shows (see ‘2.6 Approximate ground state’ [21]) that when the in-plane applied magnetic field is collinear to the in-plane projections of any one of the six components of these $\vec{Q}_{T_{1g}}$ vectors, it immediately couples to the octupoles by reorienting the spin-configuration into one of the equivalent (111) planes as shown in Fig. 1(c). This coupling provides direct access to the out-of-plane projection of $\vec{Q}_{T_{1g}}$ which can lead to an AHE as per equation (1) when electrical measurements are performed in the plane. Due to this, one expects a 120° angular dependence of the measured AHE as theoretically calculated in Fig. 1(d). We point out here that we plot all components of the $\vec{Q}_{T_{1g}}$ vector in Fig. 1(d) and find that its dependence on the magnetic field resembles that of the magnetization, $\vec{M}_{T_{1g}}$, which illustrates its role as a fictitious magnetization; however, the key difference is that the octupole produces finite contributions to the in-plane AHE, unlike $\vec{M}_{T_{1g}}$. This defines a distinct difference from the conventional (dipole-driven) AHE in a FM as the AHE is not allowed to occur when electrical measurements and applied magnetic field are coplanar.

In addition, our theoretical calculations suggest a third term in equation (1) that predicts a nontrivial Hall effect originating from the scalar chirality of the spin textures. Such a quantity was first discussed in high temperature superconductors [23, 24] when considering contributions to the Hall conductivity, whose underlying physics can similarly be attributed to the THE in a skyrmion [17–20, 25]. This can be observed in the low field regime when the spins reorient, maximizing the scalar spin chirality.

2 Experimental Results

To test these theoretical predictions, Mn_3NiCuN (111) thin film of 20 nm thickness are grown on an MgO (111) substrate, and then capped with a 3 nm thin Pt layer to prevent oxidation. After the thin film growth, Hall bar devices were patterned on the (111) kagome plane as shown in Fig. 2(g). The details of the sample preparation can be found in the method section and in reference [22]. First, we verify the presence of the $\vec{Q}_{T_{1g}}$ component’s contribution to the AHE signal by measuring the standard Hall effect in the kagome plane while sweeping the magnetic field out-of-plane field along the [111] direction (z-axis) at 100 K, well below the Néel temperature ($T_N \sim 200$ K) [22]. The longitudinal resistivity of the film is $\sim 150 \mu\Omega\text{cm}^{-1}$ at a temperature 100 K. Fig. 2(a) shows the measured AHE data for the z-field sweep that can be fitted by using $R_{xy} = A \tanh(B)$. We also verify that this AHE signal disappears above the Néel temperature (see Fig. S2(b) in ‘1.1 Sample characterization’ [21]). This result is consistent within the framework of the octupole moment ($\vec{Q}_{T_{1g}}$) induced AHE (equation (1), first term), but additionally a small magnetic moment is also present in our system (see Fig. S2(a) in ‘1.1 Sample characterization’ [21]), meaning that the magnetic dipole component ($\vec{M}_{T_{1g}}$) also contributes to the AHE. The measured anomalous Hall resistance (R_{xy}) is comparable to the previous reports [8, 9, 26, 27].

Now we perform the measurements of transverse resistance on the (111) plane while sweeping the magnetic field in the plane along different in-plane crystallographic

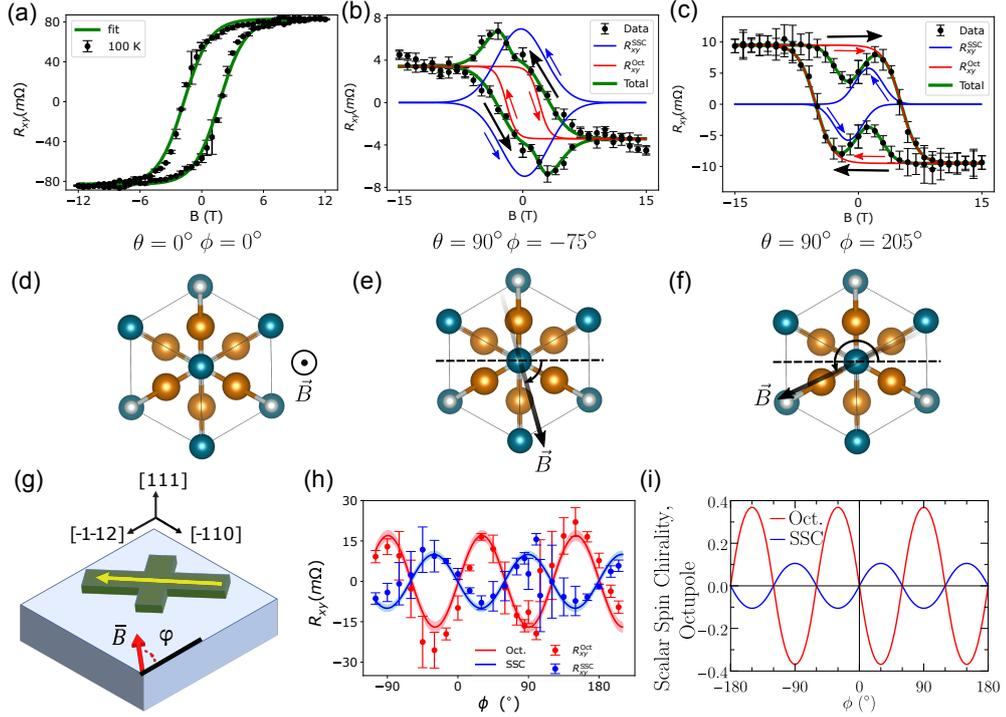


Fig. 2 (a)-(c) The measured Hall resistance as a function of applied magnetic field out of the kagome plane (a) and within the kagome plane along two different crystallographic angles, $\phi = -75^\circ$ (b) and $\phi = 205^\circ$ (c). (d)-(f) Schematics of the direction of the applied B field corresponding to cases shown in (a)-(c) respectively. The black symbols are the measured values of R_{xy} in the experiment which is fit to equation (2) (green curves) using a $\tanh(B)$ function (red curves) and a Gaussian function (blue curves). Small back arrows indicate the direction of the hysteresis loop-shift. (g) Schematics of the experiment with the coordinate system. (h) Red and black points correspond to data quantified values of R_{xy}^{Oct} and R_{xy}^{SSC} fit by sinusoidal curves with 120° periodicity. (i) Theoretically determined scalar spin chirality from symmetry analysis showing the same periodicity as the octupole contribution but differing by a sign change.

directions (Figs. 2(b-c)). We observe two important features: (1) AHE-like signals, representing a step in the measured resistance, and (2) topological Hall-like (THE) signals, which are additional features only appearing in the low field regime which we will discuss later. Our data can be fitted well to equation (2),

$$R_{xy}(B) = R_{xy}^{Oct} \tanh(a(B - B_c)) + R_{xy}^{SSC} \exp(-c(B - B_0)^2), \quad (2)$$

where R_{xy}^{Oct} represents the maximum contribution coming from the octupole moment, and R_{xy}^{SSC} the maximum contribution of the scalar spin chirality, B is the magnitude of the magnetic field, B_c is the coercivity, a is related to the slope of R_{xy}^{Oct} switching, and c is related to the width of the scalar spin chirality signal.

The observation of AHE-like signal in such coplanar geometry is a nontrivial finding as it is strictly prohibited in regular FMs. However, it is a signature that applied

magnetic fields can access one of the components of $\vec{Q}_{T_{1g}}$ depending on the direction of the magnetic field-sweep with respect to the crystal axis (Figs. 1(c-d)) which is further evident following the red curve in Fig. 2(h) that exhibits a roughly 120° angular dependence, consistent with our theoretical predictions (Fig. 1). The error-bars in the data points represent the standard deviation in five different measurements.

In these experiments surprising additional features appear at low field values which can be fitted by a Gaussian function that changes sign for positive and negative applied field cycling direction. Features like these are often attributed to THE as they occur in the presence of skyrmions whose nontrivial topology can induce an emergent effective magnetic field [18, 25]. The spin textures in our system exhibit no such topology [25], however it is possible that in the low field regime the spins rotate out of their coplanar orientation and maximize the scalar spin chirality ($\vec{S}_i \cdot (\vec{S}_j \times \vec{S}_k)$) [17] thereby producing THE-like signals as predicted by the third term in equation (1). A consequence of this is that for certain ϕ where the THE-like component is larger than the $\vec{Q}_{T_{1g}}$ component, R_{xy} switches before B changes polarity as shown in Fig. 2(b) for $\phi = -75^\circ$. This would be thermodynamically prohibited if the AHE has contributions only from $\vec{Q}_{T_{1g}}$ or $\vec{M}_{T_{1g}}$. To verify the source of the additional contribution, we compute the components of the scalar spin chirality by parameterizing a free energy expression of the irreducible representations with first principles calculations and solve a Landau-Lifshitz-Gilbert equation to provide the dependence of the scalar spin chirality ($\vec{S}_i \cdot (\vec{S}_j \times \vec{S}_k)$) and octupole ($\vec{Q}_{T_{1g}}$) moment as a function of in-plane magnetic field angle ϕ . The simulation suggests that the non-coplanar spin-textures are possible and predicts that both the octupole signal (arising from $\vec{Q}_{T_{1g}}$) and the THE-like signal (arising from $\vec{S}_i \cdot (\vec{S}_j \times \vec{S}_k)$) possess an angular dependence with 120° rotational symmetry (Fig. 2(i)). This result is qualitatively consistent with the angular dependence of the both the signals in our experiment (Fig. 2(h)) complete with their opposing signs.

3 Discussion and Conclusion

Whilst attempts have been made to quantify the behavior of the complex spin structures present in NC-AFMs using simple pictures to explain the sign change, for example, in the AHE [5–9, 28–36], our work provides a full understanding of the signal of the AHE as a function of the magnetic field. Our analysis of the underlying spin dynamics elucidates a clear interplay of coexisting orders within a noncollinear antiferromagnet, which sets this class of magnetic order apart from conventional ferromagnets and antiferromagnets. These collinear spin structures host only one order parameter apiece, the magnetization and the Néel vector, whereas noncollinear antiferromagnets exhibit further complexities that have direct consequences on the AHE that can only be understood through expansion in local spins beyond the ferromagnetic case. For Mn_3NiCuN , and subsequently the whole class of Mn_3XY compounds, one can uncover the coexistence of three distinct orders: the magnetization, a quantity in part responsible for the conventional AHE in this NC-AFM, the octupole contribution, that provides both conventional and also in-plane AHE contributions and finally the THE-like component generated when the spins are non-coplanar. Although this

particular material is merely a prototypical example of the vast array of other NC-AFM orders, we present a very clear paradigm shift in the way these materials are to be viewed: that they have multiple unconventional order parameters which behave like a magnetization, yet they affect the Hall transport in unique ways.

In summary, we systematically study the symmetry of the transverse Hall resistance in Mn_3NiCuN (111) by applying magnetic fields in the kagome plane along related crystallographic directions. We find that whenever the external applied magnetic field is collinear to the in-plane projections of any one of the octupoles, an AHE can be detected even in the limit of vanishing magnetization. The six octupoles that have in-plane components lead to a 120° symmetric AHE signal even when magnetic field and electrical measurements are coplanar, a remarkable contrast from the conventional AHE in FMs. We observe THE-like features and decompose the signal into octupole and THE-like components, finding the THE-like components to behave with a similar 120° angular dependence as the octupole component while sweeping the magnetic field in the kagome plane. We attribute this effect to a scalar-chirality emerging during the spin-reorientation at low magnetic fields. Our experimental results are well supported by theoretical predictions. Our work represents a significant step in uncovering the complex, non-trivial phenomena in NC-AFMs, greatly enhancing the understanding of the octupole moments, and distilling the complex spin textures into clear, coexisting orders. This understanding opens the possibility to explore multiple means to harness NC-AFMs for novel spintronic technological applications.

Acknowledgments. We acknowledge funding from King Abdullah University of Science and Technology (KAUST) under award 2020 – CRG8 – 4048. A.M was supported by the Excellence Initiative of Aix-Marseille University - A*MIDex, a French "Investissements d'Avenir program". In addition, the Deutsche Forschungsgemeinschaft (DFG, German Research Foundation) – Grant No. TRR 173/2 – 268565370 Spin+X (projects A01, BO2 and A11). A.R, B.B, L.L.D and M.K acknowledge funding from the European Union's Framework Programme for Research and Innovation Horizon 2020 (2014 – 2020) under the Marie Skłodowska-Curie Grant Agreement No. 860060 (ITN MagnEFi). Y.M., J.S., W.F., and Y.Y. acknowledge the funding under the Joint Sino-German Research Projects (Chinese Grant No. 12061131002 and German Grant No. 1731/10-1) and the Sino-German Mobility Programme (Grant No. M-0142). R.Y.D. and L.L-D. acknowledge funding from Spanish "Ministerio de Ciencia e Innovacion" under project PID2020-117024GD-C41. T.G.S., F.R.L., D.G. and Y.M. gratefully acknowledge the Jülich Supercomputing Centre for providing computational resources under project jiff40. T.H and H.A acknowledge funding from the Japan Society for the Promotion of Science (KAKENHI Grant Nos. 20H02602 and 19K15445).

3.1 Contributions

Adithya Rajan performed the experimental measurements, Tom G. Saunderson performed the first principles calculations and wrote the paper with Adithya Rajan and Arnab Bose. Fabian R. Lux performed the symmetry analysis, Rocío Yanes Díaz and Luis López-Díaz performed atomistic spin dynamics simulations. Hasan M. Abdullah

performed tight binding calculations and provided insights on the scalar spin chirality with Gokaran Shukla, Udo Schwingenschlögl and Aurélien Manchon. Jun-Young Kim assisted in the experimental discussions, Tetsuya Hajiri and Hidefumi Asano performed thin film sample deposition, Beatrice Bednarz assisted with device fabrication. Yugui You, Wangxiang Feng, Yuriy Mokrousov and Dongwook Go provided insights in the transport from the first principles perspective, Olena Gomonay and Jairo Sinova provided insights on the symmetry analysis. Tom G. Saunderson, Fabian R. Lux and Yuriy Mokrousov coordinated the theory effort. Mathias Kläui provided experimental insight and has been the principal investigator, supervising the whole project.

3.2 Corresponding author

Correspondence to Mathias Kläui.

4 Ethics declarations

4.1 Conflict of Interest

The Authors declare that there is no conflict of interest.

5 Methods

5.1 Material and Device fabrication

On MgO (111) substrate, 20 nm Mn_3NiCuN thin film was deposited using reactive magnetron sputtering at 375 °C substrate temperature under 2.0 Pa with 4% N_2 + 96% Ar gas mixtures. After growth, the sample was annealed in-situ at 500°C under the same atmosphere as film growth. Please refer to [22] for further details on thin film deposition. A 3 nm Pt layer was deposited in-situ to prevent oxidation. Epitaxial Mn_3NiCuN growth was confirmed by X-ray diffraction measurements with Cu K_α radiation (See Fig. S1 ‘1.1 Sample characterization’ in the Supplementary [21]). After the thin film growth, Hall bar devices with current line of width 10 μm and voltage line of width 3 μm were patterned using electron beam lithography, and the surrounding area removed using Ar^+ ion etching.

5.2 Transport measurements

The sample with patterned Hall bars was mounted on a standard PCB with Au contacts contacted to the Hall bars by wire bonding using TPT Hybond 572-40. The PCB with contacted sample was then mounted on attocube ANRv51/RES piezo-controlled rotatable sample holder which was inserted in a variable temperature cryostat from Oxford Instruments to perform magneto-transport measurements. Keithley 2400 was used as a current source, and the Hall voltage was measured using Keithley 2182A nano-voltmeter.

5.3 Data processing

The acquired Hall signal was anti-symmetrized ($R_{xy}(B) = (V_{xy}(B) - V_{xy}(-B))/2I_{xx}$) to extract the anomalous Hall effect, and to remove any contributions from the longitudinal signal. The anomalous Hall signal was centered and the contribution linear with B corresponding to the ordinary Hall effect subtracted. The planar hall effect was also analyzed and removed in Fig. S3 and is plotted in Fig. S4 in section ‘1.2 Data processing’ of the supplementary [21].

5.4 Computational details

We performed Density Functional Theory calculations for bulk Mn_3NiCuN using the experimental lattice constant 3.9012\AA from Zhao *et al* [22]. We perform calculations using the FLEUR code [37] which implements the full potential linear augmented plane wave method (FP-LAPW) [38], employing the generalized gradient approximation (GGA) [39]. In order to parameterize the symmetry analysis, full self-consistencies were performed at multiple non-coplanar canting angles from the Υ_0 spin configuration in Fig. 1(a). In order to quantify the AHE from first principles, we employ the use of Wannier interpolation [40, 41] to efficiently compute the Berry curvature using the Kubo formalism [1]. Full details are provided in section ‘3 Numerical details’ of the supplementary information [21].

References

- [1] Nagaosa, N., Sinova, J., Onoda, S., MacDonald, A. H. & Ong, N. P. Anomalous Hall effect. *Rev. Mod. Phys.* **82**, 1539–1592 (2010).
- [2] Šmejkal, L., MacDonald, A. H., Sinova, J., Nakatsuji, S. & Jungwirth, T. Anomalous Hall antiferromagnets. *Nat. Rev. Mater.* **7**, 482–496 (2022). URL <https://www.nature.com/articles/s41578-022-00430-3>.
- [3] Chen, H., Niu, Q. & Macdonald, A. H. Anomalous hall effect arising from noncollinear antiferromagnetism. *Phys. Rev. Lett.* **112**, 017205 (2014).
- [4] Kübler, J. & Felser, C. Non-collinear antiferromagnets and the anomalous Hall effect. *Europhys. Lett.* **108**, 67001 (2014). URL <https://iopscience.iop.org/article/10.1209/0295-5075/108/67001>.
- [5] You, Y. *et al.* Anomalous Hall Effect–Like Behavior with In-Plane Magnetic Field in Noncollinear Antiferromagnetic Mn_3Sn Films. *Adv. Electron. Mater.* **5**, 1800818 (2019). URL <https://onlinelibrary.wiley.com/doi/10.1002/aelm.201800818>.
- [6] Iwaki, H. *et al.* Large anomalous Hall effect in L12-ordered antiferromagnetic Mn_3Ir thin films. *Appl. Phys. Lett.* **116**, 022408 (2020). URL <https://aip.scitation.org/doi/abs/10.1063/1.5128241>.

- [7] Takeuchi, Y. *et al.* Chiral-spin rotation of non-collinear antiferromagnet by spin-orbit torque. *Nat. Mater.* **20**, 1364–1370 (2021). URL <https://www.nature.com/articles/s41563-021-01005-3>.
- [8] Kiyohara, N., Tomita, T. & Nakatsuji, S. Giant Anomalous Hall Effect in the Chiral Antiferromagnet Mn₃Ge. *Phys. Rev. Appl.* **5**, 064009 (2016).
- [9] Nakatsuji, S., Kiyohara, N. & Higo, T. Large anomalous Hall effect in a non-collinear antiferromagnet at room temperature. *Nature* **527**, 212–215 (2015). URL <https://www.nature.com/articles/nature15723>.
- [10] Suzuki, M. T., Koretsune, T., Ochi, M. & Arita, R. Cluster multipole theory for anomalous Hall effect in antiferromagnets. *Phys. Rev. B* **95**, 094406 (2017). URL <https://journals.aps.org/prb/abstract/10.1103/PhysRevB.95.094406>.
- [11] Kimata, M. *et al.* X-ray study of ferroic octupole order producing anomalous Hall effect. *Nat. Commun.* **12**, 5582 (2021). URL <https://www.nature.com/articles/s41467-021-25834-7>.
- [12] Johnson, F. *et al.* Identifying the octupole antiferromagnetic domain orientation in Mn₃NiN by scanning anomalous Nernst effect microscopy. *Appl. Phys. Lett.* **120**, 232402 (2022). URL <https://aip.scitation.org/doi/abs/10.1063/5.0091257>.
- [13] Lux, F. R., Freimuth, F., Blügel, S. & Mokrousov, Y. Chiral Hall Effect in Noncollinear Magnets from a Cyclic Cohomology Approach. *Phys. Rev. Lett.* **124**, 096602 (2020). URL <https://journals.aps.org/prl/abstract/10.1103/PhysRevLett.124.096602>.
- [14] Gomonaj, E. V. Magnetostriction and piezomagnetism of noncollinear antiferromagnet Mn₃NiN. *Phase Transitions* **18**, 93–101 (1989). URL <https://doi.org/10.1080/01411598908206858>.
- [15] Gomonaj, E. V. & Lvov, V. A. Phenomenological consideration of spin-wave spectrum in noncollinear antiferromagnet Mn₃NiN. *J. Magn. Magn. Mater.* **86**, 301–306 (1990).
- [16] Gurung, G., Shao, D. F., Paudel, T. R. & Tsymbal, E. Y. Anomalous Hall conductivity of noncollinear magnetic antiperovskites. *Phys. Rev. Mater.* **3**, 044409 (2019). URL <https://journals.aps.org/prmaterials/abstract/10.1103/PhysRevMaterials.3.044409>.
- [17] Martin, I. & Batista, C. D. Itinerant electron-driven chiral magnetic ordering and spontaneous quantum hall effect in triangular lattice models. *Phys. Rev. Lett.* **101**, 156402 (2008). URL <https://journals.aps.org/prl/abstract/10.1103/PhysRevLett.101.156402>.

- [18] Bruno, P., Dugaev, V. K. & Taillefumier, M. Topological Hall effect and Berry phase in magnetic nanostructures. *Phys. Rev. Lett.* **93**, 096806 (2004). URL <https://journals.aps.org/prl/abstract/10.1103/PhysRevLett.93.096806>.
- [19] Onoda, M., Tatara, G. & Nagaosa, N. Anomalous hall effect and skyrmion number in real and momentum spaces. *J. Phys. Soc. Japan* **73**, 2624–2627 (2004).
- [20] Taguchi, Y., Oohara, Y., Yoshizawa, H., Nagaosa, N. & Tokura, Y. Spin Chirality, Berry Phase, and Anomalous Hall Effect in a Frustrated Ferromagnet. *Science (80-.)*. **291**, 2573–2576 (2001). URL <https://www.science.org/doi/10.1126/science.1058161>.
- [21] See Supplemental Material, which also contains Refs. [1, 22, 37–43].
- [22] Zhao, K. *et al.* Anomalous Hall effect in the noncollinear antiferromagnetic antiperovskite $\text{Mn}_3\text{Ni}_{1-x}\text{Cu}_x\text{N}$. *Phys. Rev. B* **100**, 045109 (2019). URL <https://doi.org/10.1103/PhysRevB.100.045109>.
- [23] Wen, X. G., Wilczek, F. & Zee, A. Chiral spin states and superconductivity. *Phys. Rev. B* **39**, 11413 (1989). URL <https://journals.aps.org/prb/abstract/10.1103/PhysRevB.39.11413>.
- [24] Lee, P. A. & Nagaosa, N. Gauge theory of the normal state of high- T_c superconductors. *Phys. Rev. B* **46**, 5621 (1992). URL <https://journals.aps.org/prb/abstract/10.1103/PhysRevB.46.5621>.
- [25] Kimbell, G., Kim, C., Wu, W., Cuoco, M. & Robinson, J. W. Challenges in identifying chiral spin textures via the topological Hall effect. *Commun. Mater.* **3**, 19 (2022). URL <https://www.nature.com/articles/s43246-022-00238-2>.
- [26] Miki, R., Zhao, K., Hajiri, T., Gegenwart, P. & Asano, H. Epitaxial growth and orientation-dependent anomalous Hall effect of noncollinear antiferromagnetic $\text{Mn}_3\text{Ni}_{0.35}\text{Cu}_{0.65}\text{N}$ films. *J. Appl. Phys.* **127**, 113907 (2020). URL <https://aip.scitation.org/doi/abs/10.1063/1.5142250>.
- [27] Boldrin, D. *et al.* Anomalous Hall effect in noncollinear antiferromagnetic Mn_3NiN thin films. *Phys. Rev. Mater.* **3**, 094409 (2019). URL <https://doi.org/10.1103/PhysRevMaterials.3.094409>.
- [28] Kimata, M. *et al.* Magnetic and magnetic inverse spin Hall effects in a non-collinear antiferromagnet. *Nature* **565**, 627–630 (2019). URL <https://doi.org/10.1038/s41586-018-0853-0>.
- [29] Nan, T. *et al.* Controlling spin current polarization through non-collinear antiferromagnetism. *Nat. Commun.* **11**, 4671 (2020). URL <https://www.nature.com/articles/s41467-020-17999-4>.

- [30] Xie, H. *et al.* Magnetization switching in polycrystalline Mn₃Sn thin film induced by self-generated spin-polarized current. *Nat. Commun.* 2022 **13**, 5744 (2022). URL <https://www.nature.com/articles/s41467-022-33345-2>.
- [31] Chen, X. *et al.* Octupole-driven magnetoresistance in an antiferromagnetic tunnel junction. *Nature* **613**, 490–495 (2023). URL <https://www.nature.com/articles/s41586-022-05463-w>.
- [32] Qin, P. *et al.* Room-temperature magnetoresistance in an all-antiferromagnetic tunnel junction. *Nature* **613**, 485–489 (2023). URL <https://www.nature.com/articles/s41586-022-05461-y>.
- [33] Holanda, J. *et al.* Magnetic Damping Modulation in IrMn₃/Ni₈₀Fe₂₀ via the Magnetic Spin Hall Effect. *Phys. Rev. Lett.* **124**, 087204 (2020). URL <https://journals.aps.org/prl/abstract/10.1103/PhysRevLett.124.087204>.
- [34] Zhang, W. *et al.* Giant facet-dependent spin-orbit torque and spin Hall conductivity in the triangular antiferromagnet IrMn₃. *Sci. Adv.* **2**, e1600759 (2016). URL <https://www.science.org/doi/10.1126/sciadv.1600759>.
- [35] Reichlova, H. *et al.* Imaging and writing magnetic domains in the non-collinear antiferromagnet Mn₃Sn. *Nat. Commun.* **10**, 5459 (2019). URL <https://www.nature.com/articles/s41467-019-13391-z>.
- [36] Rout, P. K., Madduri, P. V., Manna, S. K. & Nayak, A. K. Field-induced topological Hall effect in the noncoplanar triangular antiferromagnetic geometry of Mn₃Sn. *Phys. Rev. B* **99**, 094430 (2019). URL <https://journals.aps.org/prb/abstract/10.1103/PhysRevB.99.094430>.
- [37] For the program description, see <https://www.flapw.de>.
- [38] Wimmer, E., Krakauer, H., Weinert, M. & Freeman, A. J. Full-potential self-consistent linearized-augmented-plane-wave method for calculating the electronic structure of molecules and surfaces: O₂ molecule. *Phys. Rev. B* **24**, 864–875 (1981).
- [39] Perdew, J. P., Burke, K. & Ernzerhof, M. Generalized Gradient Approximation Made Simple. *Phys. Rev. Lett.* **77**, 3865–3868 (1996). URL <http://www.ncbi.nlm.nih.gov/pubmed/10062328%5Chttp://link.aps.org/doi/10.1103/PhysRevLett.77.3865%5Chttp://link.aps.org/abstract/PRL/v77/p3865>.
- [40] Freimuth, F., Mokrousov, Y., Wortmann, D., Heinze, S. & Blügel, S. Maximally localized Wannier functions within the FLAPW formalism. *Phys. Rev. B - Condens. Matter Mater. Phys.* **78**, 035120 (2008).
- [41] Pizzi, G. *et al.* Wannier90 as a community code: New features and applications. *J. Phys. Condens. Matter* **32**, 165902 (2020).

- [42] Wang, X., Yates, J. R., Souza, I. & Vanderbilt, D. Ab initio calculation of the anomalous Hall conductivity by Wannier interpolation. *Phys. Rev. B - Condens. Matter Mater. Phys.* **74**, 195118 (2006).
- [43] Ky, V. D. Planar Hall Effect in Ferromagnetic Films. *Phys. status solidi* **26**, 565–569 (1968).